THE AMERICAN SOCIETY OF MECHANICAL ENGINEERS
345 E. 47th St., New York, N.Y. 10017

94-GT-46

SUPPRESSION OF SECONDARY FLOWS IN A MIXED-FLOW PUMP IMPELLER BY APPLICATION OF 3D INVERSE DESIGN METHOD: PART 2 – EXPERIMENTAL VALIDATION

A. Goto and T. Takemura
Ebara Research Company, Limited
Fujisawa-shi, Japan

M. Zangeneh
Department of Mechanical Engineering
University College of London
London, United Kingdom

Abstract

In Part I of this paper, a mixed-flow pump impeller was designed by a fully three-dimensional inverse design method, aimed at suppressing the secondary flows on the blade suction surface. In this part, the internal flow fields of the impeller are investigated experimentally, using flow visualization and phase-locked measurements of the impeller exit flow, in order to validate the effects of secondary flow suppression. The flow fields are compared with those of a conventional impeller, and it is confirmed that the secondary flows on the blade suction surface are well suppressed and the uniformity of the exit flow fields is improved substantially, in both circumferential and spanwise directions. The effects of tip clearance and the number of blades for the inverse designed impeller are also investigated experimentally and numerically.

Nomenclature

H	head (m)
l	meridional blade chord length
LE	impeller leading edge
Q	flow rate (m^3 / sec)
Q*	flow rate ratio = Q /(Q at design point)
r	radius
TE	impeller trailing edge
U	peripheral blade speed
W	relative velocity
β	blade angle measured from circumferential direction
Ω	angular rotation frequency (radian / sec)

Subscripts

1	inlet
2	exit
m	midspan
t	blade tip

Introduction

It is well acknowledged that secondary flows have dominating effects in establishing exit flow non-uniformity of centrifugal and mixed-flow turbomachinery impellers. The secondary flow pattern inside the impeller not only affects the performance and the stability of the impeller itself, but also the performance of the downstream diffuser, which accepts the impeller discharge flow. Goto (1992a) studied the process of the jet-wake flow formation by secondary flows, inside an isolated mixed-flow pump impeller at various tip clearances, based on experimental observations and numerical computations. The link between the jet-wake flow pattern and the onset of the positively sloped head-flow characteristics (stall onset) was also investigated by Goto (1992b), and it was found that impellers stalled at higher flow rates when the wake regions located closer to the casing-suction surface corner.

In Part 1 of this paper (Zangeneh et al., 1994), a mixed-flow pump impeller was designed by a fully three-dimensional inverse design method, aimed at suppressing the secondary flows on the blade suction surface. Numerical computation by the Dawes Navier-Stokes code predicted well-suppressed secondary flows on the blade suction surface, and substantial improvement in the exit flow field were achieved compared to the predicted flow fields of a corresponding conventional impeller.

In Part 2 of the present paper, the internal flow fields of the impeller are investigated experimentally in order to validate the effectiveness of the three-dimensional inverse design method. The flow fields are compared with those of a conventional impeller, and the secondary flow suppression and the uniformity of the exit flow fields are discussed. The effects of tip clearance and the number of blades for the inverse designed impeller are also discussed.

Experimental Apparatus and Method

Test Loop

Figure 1 schematically shows the cross section of a mixed-flow pump stage used for performance tests and flow field measurements.

Presented at the International Gas Turbine and Aeroengine Congress and Exposition
The Hague, Netherlands – June 13–16, 1994
This paper has been accepted for publication in the Transactions of the ASME
Discussion of it will be accepted at ASME Headquarters until September 30, 1994

Table 1 Design Specification

	hub / midspan / shroud	Design flow rate : 9.2 m^3 / min
r_1 (mm)	58.0 / 102.3 / 132.5	Design pump head : 6.5 mH_2O
r_2 (mm)	142.5 / 157.8 / 171.7	Rotational speed : 800 rev / min

The inlet of the diffuser blades were moved to the downstream location away from the trailing edge of the impeller in order to measure the impeller exit flows at Station B under the isolated impeller configuration. Experiments were carried out on both the inverse designed impeller and the corresponding conventional impeller. The design specific speed of the pump was $\Omega\cdot\sqrt{Q}/(gH)^{3/4}$=1.34, i.e. 550 (rpm,$m^3$/min,m). Water was used as the test fluid and the pump stage was placed in a closed flow loop consisting of a 440-mm-dia suction pipe, a 350-mm-dia delivery pipe, a 10.3-m^3 reservoir tank, and a return line with venturi tubes and throttles. Performance tests were conducted according to ISO standards. The impeller speed was 800 rpm giving a Reynolds number of $Re = W_1 l_m / \nu = 1.33 \times 10^6$ at the design point.

Model Impellers

Each blade of the inverse designed impeller was manufactured from a block of bronze material by a 5-axis numerically controlled milling machine, and thus manufactured 7 blades were stacked into a hub to form a 7 bladed impeller. The impeller was also tested under a 5 bladed configuration by replacing the hub. The front shroud was removable and so the effects of the tip leakage flow were also examined experimentally. The blade tip clearance was 0.5mm in all unshrouded cases including conventional impeller case. The design criteria and specifications were described in detail in Part 1 of this paper (Zangeneh et al., 1994). In contrast, the corresponding conventional impeller was designed as a 5 bladed impeller by simply connecting the inlet and the exit blade angles with a smooth monotonic curve on each stream surface. The conventional impeller was made by casting and the blade surface finish was applied to make the flow passage hydrodynamically smooth. The unshrouded conventional impeller was made by removing the front shroud by machining. The meridional geometries of the inverse designed and conventional impellers were identical, apart from the curved leading edge in the conventional impeller which was replaced by a straight line connecting the hub and shroud in the inverse design. The meridional geometry and design conditions are given in Table 1, and the test cases are summarized in Table 2. Here, suffix "u" represents the unshrouded case, "s" the shrouded case, "5" the five bladed case, and "7" the seven bladed case.

Figure 2 compares the geometry of the inverse designed impeller (CII-u5) with that of the conventional impeller(O-u5) under 5 bladed unshrouded configuration. The trailing edge of the inverse designed impeller is inclined in the counter-rotating direction towards the tip, and the effect of the stacking condition adapted in this particular design is clearly observed. As was discussed in Part 1 of the paper, the spanwise gradients of reduced static pressure are well correlated with the presence of meridional secondary flows (also see Cumpsty, 1989). The blade lean of CII impeller reduced the blade loading near the tip and increased the loading at the hub. Because of this, the spanwise gradients of reduced static pressure were reduced and it was possible to suppress the spanwise secondary flows on the blade suction surface. On the other hand, the blade lean of the conventional impeller is in the opposite direction, although there is no clear hydrodynamic background in this case. Table 3 shows the absolute difference in blade angles between these two impellers at three different locations. The difference in blade angle is quite substantial, and it is easily understood that such blade shape can never be reached by conventional design hypothesis.

Flow Field Measurements and Flow Visualization

Besides the performance tests, inlet and exit flow measurements of the impeller were carried out using two types of pressure probes.

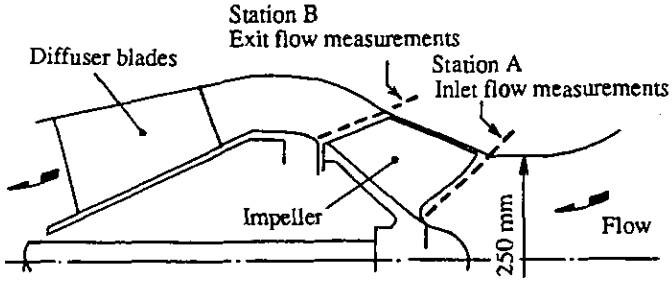

Fig.1 Cross section of mixed-flow pump stage

Table 2 Test Cases

Test Case	Blade Number	Performance Tests	Flow Visualization	Exit Flow Measurements
O-s5	5	X		
O-u5	5	X	X	X
CII-s7	7	X	X	X
CII-u7	7	X	X	X
CII-u5	5	X		X

O: Conventional Design CII: Inverse Design
s: Shrouded u: Unshrouded

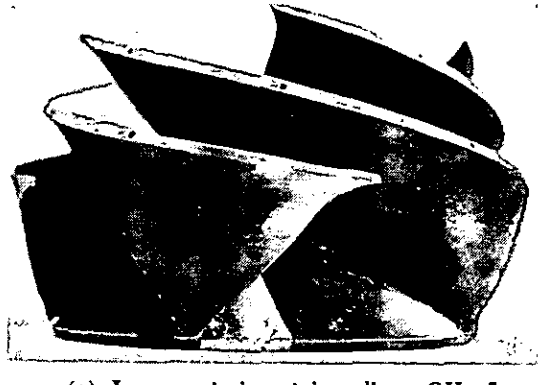

(a) Inverse designed impeller CII-u5

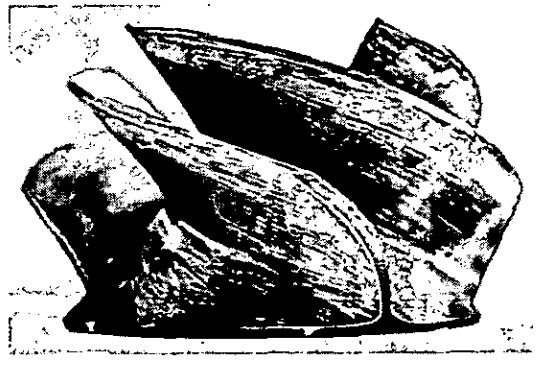

(b) Conventional impeller O-u5

Fig.2 Comparison of impeller configuration

The inlet flow was measured by an ordinary 3-hole Pitot probe at Station A, and the relative exit flow was measured by a two-hole Pitot probe with high frequency response at Station B (Fig.1), 8mm downstream of the trailing edge. In the latter probe, two diffusion type semi-conductor pressure transducers were placed in the stem tube. The resonance frequency of the pressure sensing system was about 5.6kHz and was high enough compared with the blade passing frequency of 67 Hz at 800 rpm. Three-dimensional relative flow fields at the impeller exit were measured by the phase-locked multi-sampling and averaging technique (For details on the measuring system, the data reduction method, and the accuracy of measurements, see Goto, 1988).

In order to assess the magnitude of the secondary flows within the impellers, flow visualization of the wall streamlines was carried out using an oil-film technique. The viscosity of the oil was carefully adjusted, depending on the local velocity on the flow passage walls, to get clear pictures of the flow pattern.

Accuracy of Measurements

The probable uncertainty in the data reduction process and the measuring system of the two-hole pitot probe has been evaluated by Goto(1988) using a calibration test rig. The accuracy is ±2.5% in the static pressure, ±1.3% in the velocity, ±0.3 degrees in the yaw angle, and ±1 degree in the pitch angle. It has also been confirmed that the steady state calibration curves are correctly applicable to the present unsteady flow.

The flow rates obtained by the integration of measured velocity fields agreed with those obtained by the venturi tubes at an accuracy of ±5% in all cases presented in this paper.

Discussion on Numerical Results

In Part 1 of this paper, the inverse designed impeller CII was designed as a 7 bladed shrouded impeller (CII-s7). In the following experimental investigations, impeller CII was tested with and without the shroud, and under 7 and 5 bladed configuration in order to see the effects of the tip clearance and the difference in blade numbers. In the present section, the effects of the tip clearance and the reduction in the blade number are numerically investigated beforehand, based on the computations by an incompressible version of the Dawes 3-D Navier-Stokes code (Walker and Dawes, 1990) at the design operating condition. Goto (1992a) applied the Dawes code to the present conventional impeller O at various tip clearances, including the shrouded case, and compared the predicted jet-wake flow pattern with that in experiments at the exit of the impeller. The results show that the Dawes code can capture the characteristic feature of the difference in the secondary flow pattern and the resulting jet-wake flow development inside the impeller.

Effects of Tip Clearance

The present three-dimensional inverse design method does not take into account the effects of tip clearance. However, both shrouded and unshrouded impellers are widely used, and there are also a number of literatures which show the dominating influence of the tip leakage flow on the three-dimensional flow pattern, such as a jet-wake flow formation pattern.

The Dawes code was applied to compare the secondary flow pattern between the unshrouded CII impeller (CII-u7) and the unshrouded conventional impeller O-u5. Figure 3 shows the computational grid for CII-u7 with a tip clearance of 0.5mm. The grid points were clustered near the endwalls and blade surfaces, and the blade tip was rounded off in the simulation. There were only two meshes in the clearance, but this should be enough to capture the global effects of the tip leakage flow. The grid size of 29 x 125 x 29 (pitchwise x streamwise x spanwise) required about 10 hours of CPU time on a single processor of a Convex C220 computer (100MFlops).

Figure 4 compares the secondary flow pattern between CII-u7 and O-u5 impellers on the meridional plane close to the blade suction surface. The relative velocity contours at two different streamwise locations, on quasi-orthogonal planes at 50%-chord and the trailing

Table 3 Absolute difference in blade angles
$= |\beta_{CII} - \beta_{Conventional}|$

Location	Shroud	Hub
8%-chord	1.7	2.4
50%-chord	7.3	1.6
92%-chord	10.3	17.8

(degree)

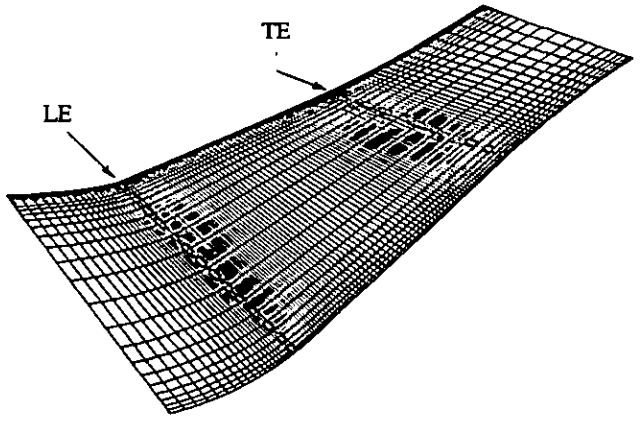

Fig.3 Computational grid on Meridional Plane
(case CII-u7, grid size=29x125x29)

edge, are also presented. The secondary flows, on the blade suction surface of CII, were better suppressed than those of the unshrouded conventional impeller (Fig.4c), and the exit flow was fairly uniform in the spanwise direction. In the case of O-u5, the non-uniformity of the exit flow fields was not as unfavorable as that of the shrouded case O-s5, presented in Part 1 of this paper. This was considered to be caused by the positive effects of the tip leakage flow. However, the non-uniformity of the exit flow fields still existed near the casing, and this may adversely affect not only the efficiency and the stability of the impeller but also the performance of the downstream diffuser, which accepts the impeller exit flow. At 50%-chord location (Fig.4a), there appeared low relative velocity region close to the casing due to the tip leakage vortex in both CII-u7 and O-u5. However, at the trailing edge plane (Fig.4b), the casing viscous region is thinner in CII-u7. This is considered to be the effects of secondary flow suppression in CII-u7. Overall, the present computations show very little effects by the tip leakage vortex on the suppression of secondary flows on the blade suction surface.

Effects of Blade Number

Figure 4b shows much thicker blade boundary layer in CII-u7, between 25%-span and the blade tip. The inverse designed impeller had 7 blades and the blade angle was much lower than that of the conventional impeller in the tip region. These two factors made the effective passage area of CII-u7 very narrow. In addition to this, the blade length was longer in CII at the tip due to the small blade angle. Because of this, more friction losses could be generated in CII-u7, and made the blade boundary layer thicker towards the blade tip. It was felt unfair to compare the internal flows between the 7 bladed inverse designed impeller and those of the conventional impeller, originally designed under the 5 bladed configuration. So, it was decided to do additional experiments for CII with reduced blade number of 5, although this could have deteriorated the secondary flow suppression effects. In this paragraph, the effect of the reduction in blade number is discussed based on numerical predictions.

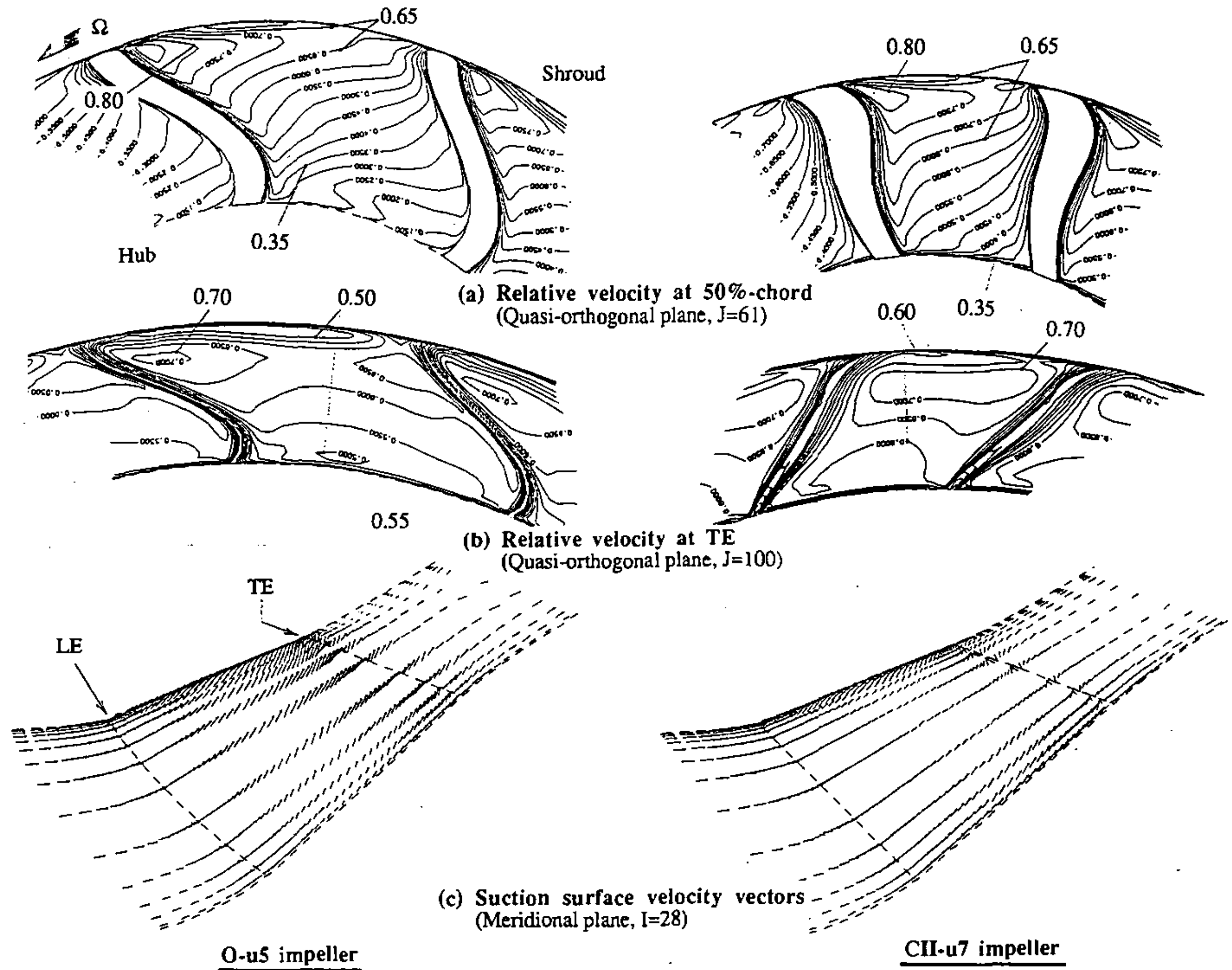

Fig.4 Comparison of predicted flow patterns for unshoruded cases CII-u7 and O-u5
(Contour interval = 0.05, Normarized by U_{2m})

Figure 5 compares the relative velocity contours between CII-s7 and CII-s5 at two different streamwise locations, on quasi-orthogonal planes at 50%-chord and the trailing edge. The secondary flow pattern on the meridional plane close to the blade suction surface is also presented. The boundary layer thickness, relative to the pitch length, was reduced in CII-s5 because of the less blockage effects of the blade thickness. The meridional secondary flow is similar between CII-s7 and CII-s5, and their magnitude is still much weaker than that in the conventional impeller (see impeller O-u5 case in Fig.4c for example), and an uniform exit flow is achieved. In impeller CII-s5 case (Fig.5b, right), the low relative velocity region emerged to the midpitch location along the casing, compared to the case of CII-s7 (Fig.5b, left) where it stayed closer to the blade, suggesting a slight increase in the suction surface secondary flows.

The boundary layer of CII-s5 (Fig.5b, right) is still thicker than that of O-s5 (see Fig.10 of Part 1). There are probably two main causes. One is the small blade angle and the longer blade chord length at the tip of CII impeller. The blade length at the tip of CII is 1.5 times longer than that of the conventional impeller. Also the small blade angle made the effective flow passage fairly narrow, and the relative velocity was increased especially in the tip region. The other possible cause is the underestimated hydrodynamic blockage in the present inverse design (see discussion in "Overall Performance" of Part 1). Since the blockage effects were underestimated, the relative flow was accelerated in reality towards the exit and generated substantial amount of friction losses. The thick blade boundary layers may affect the impeller and the pump stage performances adversely, although the overall exit flow non-uniformity was improved in CII impeller.

Discussion on Experimental Results

Overall Characteristics

The overall performance of the pump stage with the inverse designed CII-s7 (shrouded 7 bladed) impeller was compared with that of a conventional impeller. Since the overall performance of O-s7, having the same number of blades, had not been measured, the

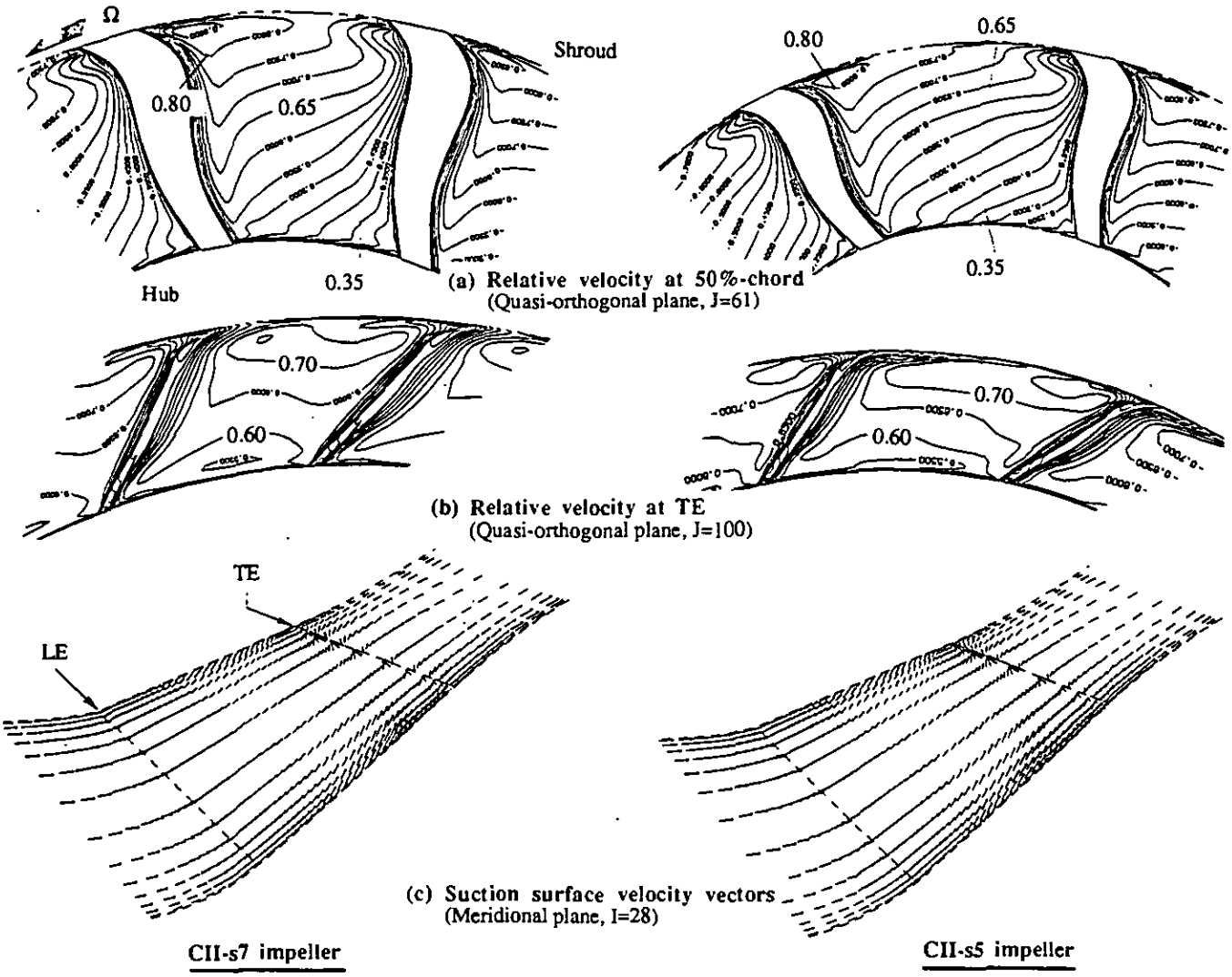

Fig.5 Comparison of predicted flow patterns for CII with different blade number
(Contour interval = 0.05, Normarized by U_{2m})

performance of O-s5 was selected for reference and compared with that of CII-s7 (Fig.6). The pump head and the shaft power were normalized by the values for O-s5 at the design point.

The pump stage with the inverse designed impeller CII-s7 showed substantially lower pump head than that of the conventional impeller O-s5 by about 15%. In the present cases, the shaft power is directly related to the impeller work input or Euler head, as the disk friction and the mechanical losses were fairly small. So, Fig.6 clearly shows that the lower head was caused by the lower impeller work input or lower Euler head of CII-s7. As was discussed in Part 1 of this paper, the main cause of this discrepancy is considered to be the blockage effects by the viscous region, developing along the flow passage walls. Since the viscous blockage effects were underestimated in the present inverse design, the relative flow inside the inverse designed impeller was accelerated in reality and the slip velocity was increased, giving lower swirl velocity inside and at the exit of the impeller. The percentage of the head reduction was larger than that of the shaft power, and so the hydraulic efficiency was also lower in the case of CII-s7. The excessive friction loss, discussed in the previous chapter, is considered to be responsible for this poor efficiency.

The stall, positively sloped head-flow characteristics, occurred late at the lower flow rate for CII-s7, and the stall margin was extended by 17 points (from Q*=0.837 to 0.665). This is possibly because of the secondary flow suppression on the suction surfaces of CII-s7 impeller blades, predicted by the numerical computations. However, since CII-s7 was lightly loaded, giving lower Euler head, the difference in the flow fields should be compared experimentally in detail in order to confirm the actual capability of the inverse design for secondary flow suppression.

Flow Visualization

In order to confirm the effects of secondary flow suppression, flow visualization was carried out for three impellers: O-u5, CII-s7 and CII-u7. Figure 7 shows the oil-film flow pattern on the blade suction surfaces at the design point. In the cases of the CII impeller, one blade among the 7 blades was taken off from the hub to make the flow pattern more visible. The streak of the oil-film flow pattern, which reached the tip of the each trailing edge, was traced in the upstream direction and the starting point at the leading edge was marked with a solid circle. The streak line reached around the root of

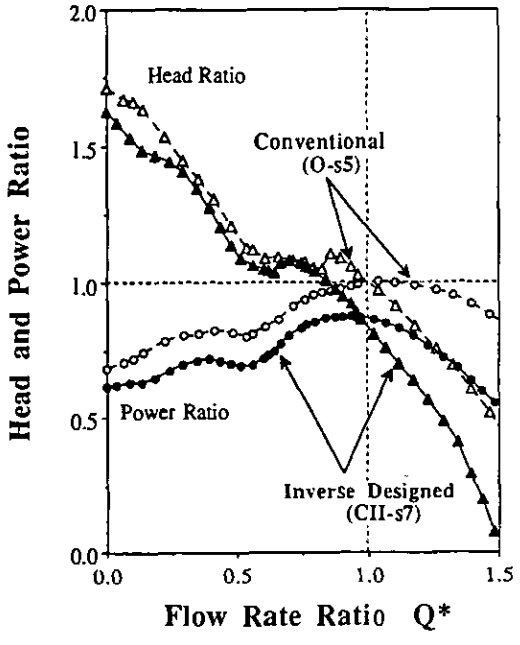

Fig.6 Comparison of measured overall performances between CII-s7 and O-s5

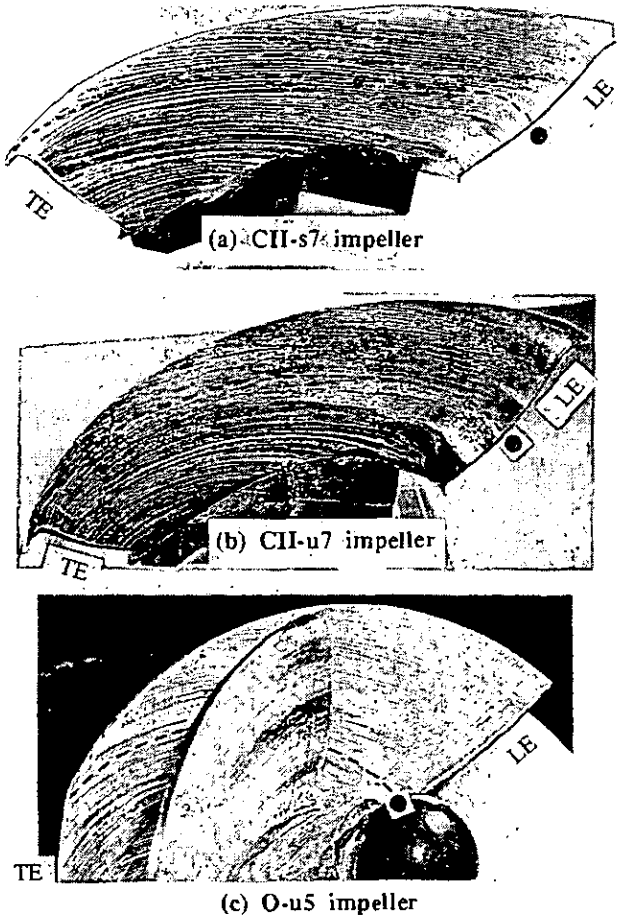

Fig.7 Comparison of oil-film flow pattern on suction surface

the leading edge in case O-u5, while it reached around the 40%-span location in both CII-s7 and CII-u7 cases. So, the secondary flows on the blade suction surfaces in cases CII-s7 and CII-u7 were relatively weak and were suppressed successfully, compared to the conventional design case O-u5.

The numerical computations for CII-s7 and CII-u7 (Fig.4c, right and Fig.5c, left) predicted fairly suppressed suction surface secondary flows compared to the case of O-u5 (Fig4c, left), showing good qualitative agreement with the measured oil-film flow patten (Fig.7). The numerical predictions, for inverse designed impellers, show increased secondary flows close to the hub surfaces between 45% and 75%-chord. This flow pattern was also observed in Fig.7a and b. Around the midspan of the inverse designed impellers, the oil-film flow pattern shows almost no secondary flow motion in the fore part region, while it was convected radially outward toward exit which was not predicted by numerical computations. This is considered to be partly because of the centrifugal force acting on the oil film due to the slight difference in specific gravity between oil and water.

The numerical computations predicted minor effects of the tip leakage flow on the suction surface secondary flows, and this was also confirmed experimentally by flow visualization. However, an

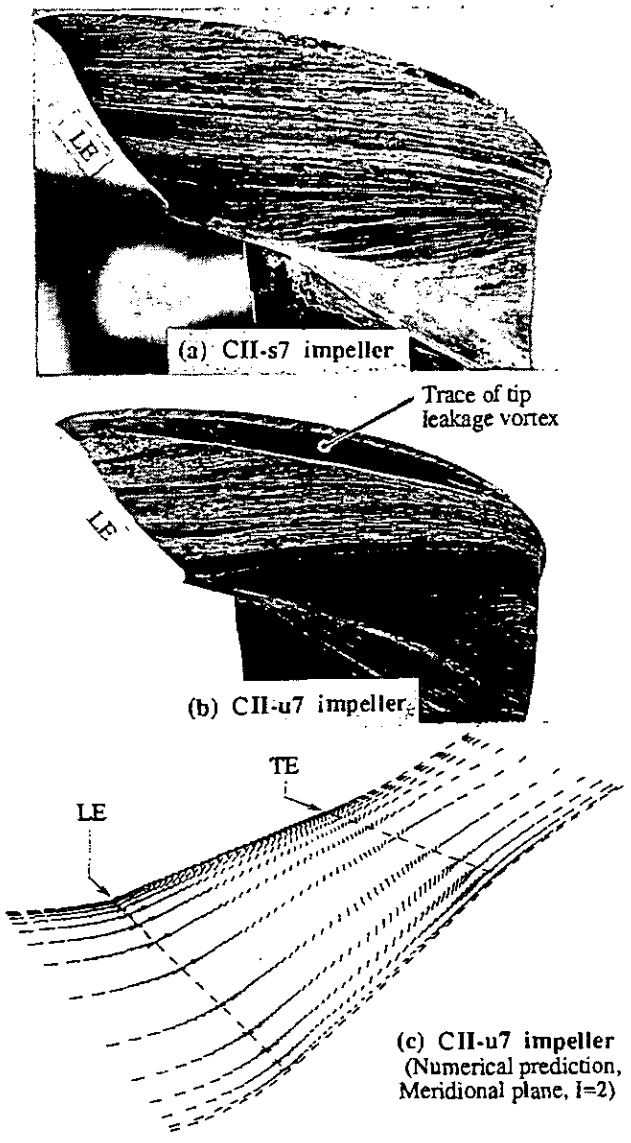

Fig.8 Comparison of secondary flow pattern on pressure surface

apparent difference was observed on the pressure surface close to the casing. Figure 8 compares the oil-film flow pattern on the pressure surfaces between CII-s7 and CII-u7. The secondary flow pattern of CII-u7, predicted by a numerical computation, is also presented. The tip leakage vortex of CII-u7 crossed over the pitch along the casing and reached to the adjacent pressure surface, showing downward movement of the oil-film flow pattern around the blade tip. The numerical computation failed to predict this phenomena possibly because of the insufficient grid number in the tip region. The predicted secondary flows were much stronger on the pressure surface than that on the suction surface, and this was confirmed by flow visualization.

Circumferentially Averaged Exit Flow

The impeller exit relative flow fields, measured by the two-hole unsteady Pitot probe, were compared among the CII-s7, CII-u7, CII-u5 and O-u5 impellers in order to see the effects of the tip clearance and the blade number. The flow loss is defined as the rothalpy difference between the measuring plane and the upstream plane of the impeller, where the flow is considered to be uniform. It was assumed that there is no inlet pre-rotation, and the inlet flow measurements showed that this assumption was correct at both Q*=1.0 and 0.85 discussed here. The inlet recirculation was not observed at Station A until the onset of the positively-sloped head-flow characteristics.

Figure 9a shows the spanwise distribution of the flow losses, mass averaged circumferentially, at the design point. The flow loss was extremely high in CII-s7 towards the shroud because of high friction loss in this region, as was discussed in the previous section. However, the loss was reduced substantially when there was a tip clearance (CII-u7). The tip clearance of 0.5mm corresponds to only 0.8% of the exit blade span height, and so a small amount of leakage flow at the tip had large effect over the whole flow fields. The loss distributions between the 65% and 20% span are identical between CII-s7 and CII-u7. The reduction of the blade number from 7 (CII-u7) to 5 (CII-u5) further reduced the flow losses between the casing and the 30%-span location. The high generation of friction losses of CII-u7 had great influence over the whole flow fields. The flow loss of CII-u5 is lower than that of the conventional impeller O-u5, especially in the outer region between the 60% and 90% span. However, the loss of CII-u5 tends to increase closer to the casing, possibly because of less effective suppression of the blade surface secondary flows, due to the reduced blade number and the resulting migration of the high loss fluid in the tip region, as was discussed in Fig.5.

Figure 9b shows the distributions at an 85% flow rate of the design point (Q*=0.85). The trend is similar to that of the design point, but the flow losses were much less in CII-u5 than those in O-u5 between the 30% and 80% span locations. The peak value of the loss in CII-s7 is lower than that of the design point (Fig.9a), since the friction loss is reduced due to the reduced flow rate and the relative velocity.

Figure 10 compares the spanwise distribution of the meridional velocity. Here, the radial and the axial components of the velocity were area-averaged in the circumferential direction. At the design point, Fig.10a, the meridional velocity distribution of CII-u5 is more uniform compared to that of the O-u5 impeller between the hub and

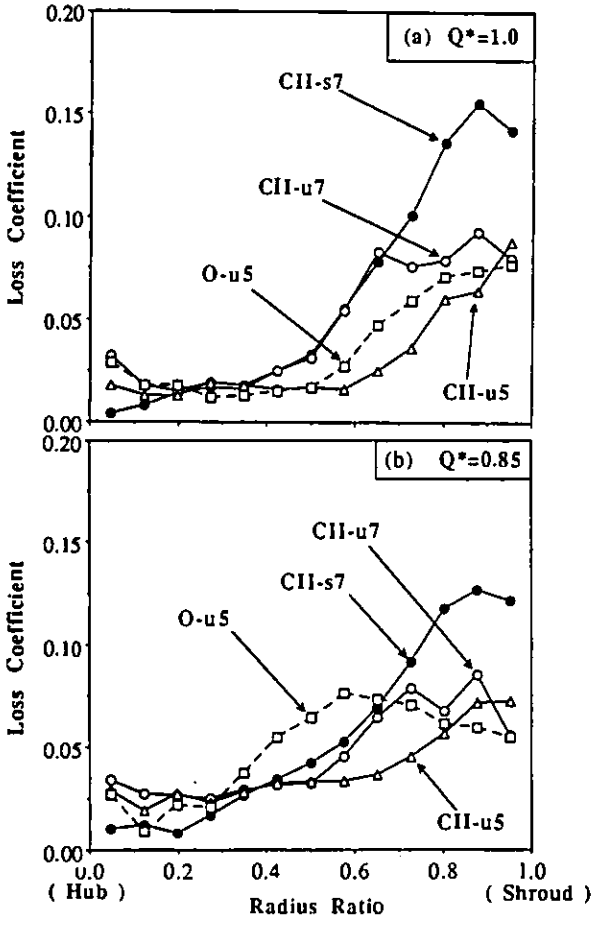

Fig.9 Measured spanwise loss distribution
(at Station B, mass-averaged circumferentially)

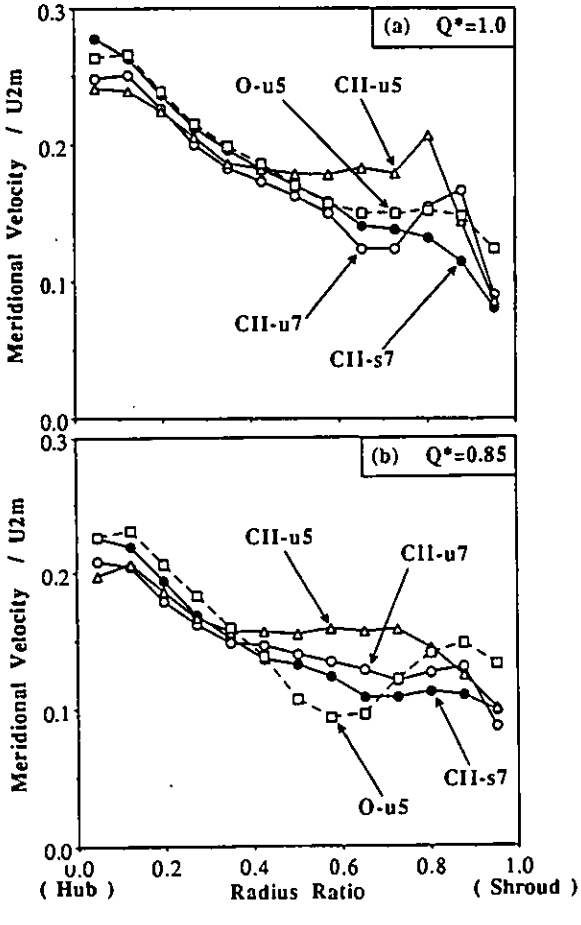

Fig.10 Measured spanwise meridional velocity distribution
(at Station B, area-averaged circumferentially)

the 80%-span location. However, the meridional velocity close to the tip becomes low in CII impellers due to high loss generation in this region. When the flow rate was reduced to Q*=0.85 (Fig.10b), meridional velocity deficit clearly increased in the O-u5 impeller between its 40% and 80% span locations, which corresponds to the high loss region in Fig.10b. The observed lower loss and more uniform meridional velocity distributions in the inverse designed impeller CII-u5 are related with the difference in secondary flow pattern inside the impeller, and this will be discussed in detail in the next paragraph

Exit Jet-Wake Flow Pattern

Figures 11 and 12 compare the measured relative velocity contours on the quasi-orthogonal planes at the exit of the impeller (Station B, Fig.1). The approximate locations of the blade trailing edges are mentioned with broken lines. The low relative velocity region of CII-s7 was extremely wide because of the excessive friction loss generated in the shroud region. When the shroud was removed (CII-u7), the flow fields near the casing were significantly improved, and further improvements were achieved when the blade number was reduced to 5 (CII-u5).

In the case of unshrouded impellers, the high loss fluid, conveyed by the suction surface secondary flows towards the tip, rolled into the tip leakage vortex. On the other hand, there was a fairly strong passage vortex around the pressure side of the passage (secondary flows from the pressure surface to the suction surface of the blade along the casing), due to the large pressure gradient generated by the Coriolis force. The wake flow, low relative velocity region, formed in the interaction region between these two vortex motions, and tended to be rolled up away from the casing (see Goto, 1992a). The flow fields of O-u5 were highly non-uniform due to thus formed jet-wake flow pattern. The region, where high loss was observed in Fig.9, corresponds to the wake flow regions in Fig.11 and Fig.12. As the flow rate was reduced, the flow fields in O-u5 became extremely non-uniform in both spanwise and pitchwise directions (Fig.12d). The strength of the suction surface secondary flows, the tip leakage vortex, and the passage vortex were all intensified at partial flow rates; the wake flow was formed further away from the casing. This is the reason of the high loss and the low meridional velocity existing between the 40% and 80%-span locations in the conventional impeller O-u5 (see Fig.9b and Fig.10b).

On the other hand, the flow fields of CII-u5 (Fig.11c) were fairly uniform in both spanwise and pitchwise directions, suggesting much weaker secondary flows on the suction surface of CII impellers. No accumulation of low relative velocity fluids was observed here. When the flow rate was reduced to Q*=0.85 (Fig.12d), there appeared a small amount of accumulation in the casing region, but the flow fields of CII-u5 still remained fairly uniform, compared to the appreciable growth in the wake flow region in the conventional O-u5 impeller.

The blade wake flows, predicted by numerical computations (Fig.4b and Fig.5b) at the trailing edge planes, have already mixed out and can not be observed in Fig.11. Although the numerical computations succeeded in predicting secondary flow pattern on blade surfaces, they failed to predict the characteristic feature of the flow fields at the exit of the impellers, such as the low relative velocity region existed widely along the casing for CII-s7, the flow field improvement in the casing region by introducing tip clearance (compare Fig.11a,b with Fig.5b and Fig.4b) and the rolling up of the wake flow in O-u5 impeller caused by the strong interaction between the tip leakage and the passage vortices.

Concluding Remarks

In Part 1 of this paper, a medium specific speed mixed-flow pump impeller was designed by a fully three-dimensional inverse design

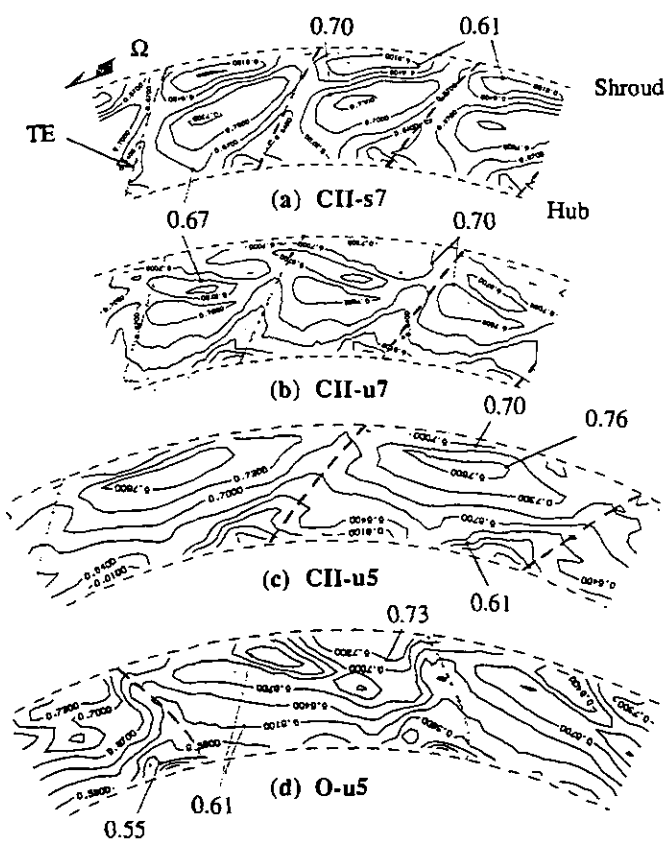

Fig.11 Measured relative exit velocity contours at Q*=1.0 (Station B, Contour interval = 0.03, Normarized by U_{2m})

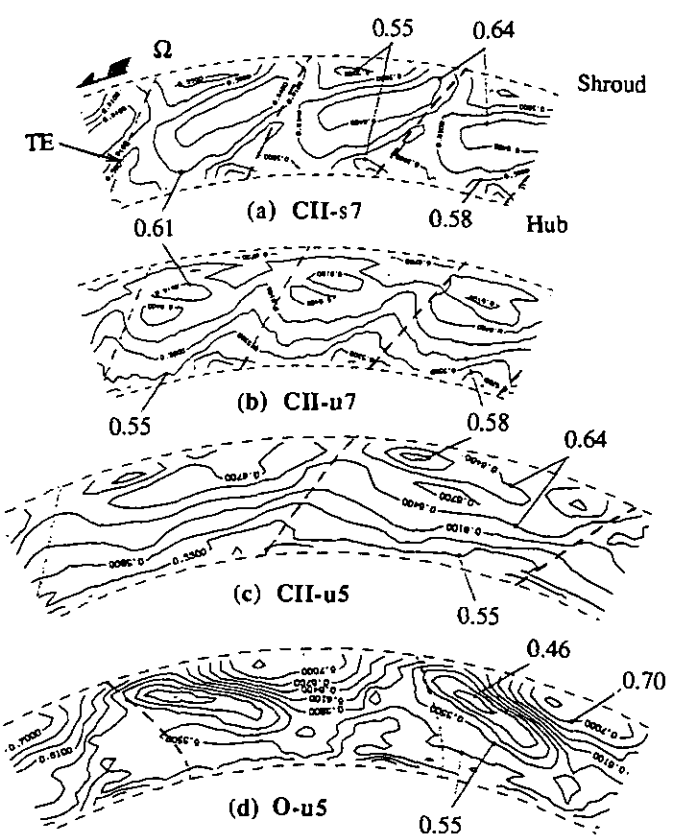

Fig.12 Measured relative exit velocity contours at Q*= 0.85 (Station B, Contour interval = 0.03, Normarized by U_{2m})

method. The objective of the design was the suppression of the secondary flows on the blade suction surface, which could be the cause of exit flow non-uniformity and the instability of the impeller. Predictions by the Dawes 3-D Navier-Stokes code showed well-suppressed blade suction surface secondary flows and fairly uniform impeller exit flow fields compared to those of the conventional impeller.

In this part, the internal flow fields of the inverse designed impeller were investigated experimentally to confirm the capability of the present three-dimensional inverse design method, especially in terms of suppression of secondary flows on the blade suction surface. The flow fields were compared with those of a corresponding conventional impeller, and it was confirmed that the secondary flows on the blade suction surface were well suppressed and the uniformity of the exit flow fields was improved substantially in both circumferential and spanwise directions.

It is well acknowledged that secondary flows play a very important role to produce the exit flow non-uniformity such as the jet-wake flow pattern at the exit of centrifugal and mixed-flow turbomachines. This phenomena often deteriorates the performance and the stability of the downstream diffuser and the stage. A substantial amount of efforts have been devoted to control secondary flows by applying a variety of empiricism, experience and more recently the iterative use of advanced CFD (computational fluid dynamics) techniques, with the expense of time and cost. The present paper showed that it is possible to control secondary flows within the impeller in a more theoretical way by the application of the three-dimensional inverse design method. It is also possible to minimize the loss generation by the careful choice of the input specification in the inverse design method, such as optimum blade number, appropriate hydrodynamic blockage and the loading distribution.

Acknowledgements

The author would like to express his deepest appreciation to Mr. T. Katsumata for his assistance in setting up the experimental apparatus and conducting the measurements. The author also would like to thank Ebara Research Co., Ltd. for permission to publish this paper.

References

Cumpsty, N.A., 1989, "Compressor Aerodynamics," Longman Scientific & Technical, pp.230-232.

Dawes, W.N., 1988, "Development of a 3D Navier-Stokes Solver for Application to all Types of Turbomachinery," ASME Paper No. 88-GT-70.

Goto, A., 1988, "Phase-locked Measurements of Three-Dimensional Periodic Flow from an Impeller Using a Two-Hole Pitot Probe," Proceedings of the 2nd International Symposium on Fluid Control and Measurements (FLUCOME '88), Sheffield, U.K., September 5-9, 1988.

Goto, A., 1992a, "Study of Internal Flows in Mixed-Flow Pump Impellers with Various Tip Clearances using Three-Dimensional Viscous Flow Computations," ASME Journal of Turbomachinery, Vol. 114, pp.373-382.

Goto, A., 1992b, "The Effect of Tip Leakage Flow on Part-Load Performance of a Mixed-Flow Pump Impeller," ASME Journal of Turbomachinery, Vol. 114, pp.383-391.

Walker, P.J. and Dawes, W.N., 1990, "The Extension and Application of Three-Dimensional Time-Marching Analyses to Incompressible Turbomachinery Flows," Transactions of the ASME, Journal of Turbomachinery, Vol. 112, pp. 385-390.

Zangeneh, M., Goto, A. and Takemura, T., 1994, "Suppression of Secondary Flows in a Mixed Flow Pump Impeller by Application of 3D Inverse Design Method. Part 1: Design and Numerical Validation," to be presented at the ASME Turbo Expo '94, Hague, June 13-16.